

1
2
3
4
5
6
7
8
9
10
11
12
13
14
15
16
17
18
19
20
21
22
23
24

**Consequences of cavity size and chemical environment
on the adsorption properties of isoreticular metal-
organic frameworks: an ~~IGC~~Inverse Gas
Chromatography study**

Inés Gutiérrez, Eva Díaz, Aurelio Vega, Salvador Ordóñez*

*Department of Chemical Engineering and Environmental Technology, University
of Oviedo, Faculty of Chemistry, Julián Clavería s/n, 33006 Oviedo, Spain
E-mail: sordonez@uniovi.es, Tel: +34 985 103 437; Fax: +34 985 103 434*

25
26
27
28
29
30
31
32
33
34
35
36
37
38
39
40
41
42
43
44
45
46
47
48
49
50
51
52

Abstract

The role of the structure of three isoreticular metal-organic frameworks (IRMOFs) on their adsorption behavior has been studied in this work, selecting different kinds of volatile organic compounds (VOCs) as adsorbates (alkanes, alkenes, cycloalkanes, aromatics and chlorinated). For this purpose, three samples (IRMOF-1, IRMOF-8 and IRMOF-10) with cubic structure and without functionalities on the organic linkers were synthesized. Adsorption capacities [at infinite dilution](#) were derived from the adsorption isotherms, whereas thermodynamic properties have been determined from chromatographic retention [data volume](#). ~~A great influence of the molecule size on both the~~ [The](#) capacity and the strength of adsorption ~~was~~ [were strongly influenced by the adsorbate size. This effect is especially relevant](#) ~~observed~~ for n-alkanes adsorption, indicating the ~~relevance~~ [key role](#) of the cavity size on this phenomenon, and hence the importance of the IRMOF structural properties. ~~A d~~ Different behavior has been observed for the polar compounds, [where](#) an enhancement on the specificity of the adsorption with the π -electron rich regions ~~being~~ [was](#) observed. This fact suggests the specific interaction of these molecules with the organic linkers of the IRMOFs.

Keywords:

Isoreticular metal-organic frameworks; Inverse gas chromatography; Adsorption properties; Surface properties; VOCs adsorption

53

54 **1. Introduction**

55 Isoreticular metal-organic frameworks (IRMOFs) are coordination polymers constituting
56 an important family of porous crystalline materials [1,2]. These materials are constituted by
57 two major components: a metal ion or metal oxide and an organic linker. The metal ions are
58 situated in vertices joined by the organic linker molecules to form the IRMOF structure [3,4].
59 The structures formed by these materials are diverse, since many different combinations of
60 metal-containing ions and the organic linkers can be made. The main features of these
61 materials are the high surface area (500 to 4 500 m²/g) [5], ~~and high~~ pore volume [6,7], as well
62 as the easiness for tuning their structure ~~[3,8]~~ by selecting the two IRMOF constituents ~~[3,8]~~.
63

64 Due to these properties, these materials are attractive candidates for a variety of
65 applications such as: storage and separation of gases (N₂, Ar, CO₂, CH₄, and H₂) [2,9-13],
66 catalysis [13-16], sensors for different molecules [13,14], and semiconductors [17]. In this way,
67 there are many published works dealing with the synthesis, characterization and gas storage
68 applications for MOFs. However, the research on the adsorption of organic molecules on this
69 type of materials is relatively scarce, in spite of their potential for this application (similar to
70 zeolites), as well as its possibility to tune both the structure and the organic linkers in order to
71 enhance the interactions between the adsorbates and the pore wall. In this way, there are just
72 few works dealing with experimental [18-21] and simulated [20,22] studies related to the
73 adsorption of organic molecules on MOFs. Furthermore, the scope of these works makes
74 difficult to compare the different results among them, since there are works focused on the
75 vapor-phase separation processes of several compounds [23], the understanding of organic
76 compounds adsorption on a selected MOF [21,24], or the adsorption of selected compounds
77 on different MOFs, with different structures and metal ions [20]. Taking into account the large
78 number of applications of adsorption processes for the separation and removal of the harmful
79 vapors of these compounds, a systematic study on the adsorption behavior of organic
80 molecules on this type of structures is of high scientific interest.

81

82 In this work, we report the adsorption of several compounds representative of volatile
83 organic compounds (VOCs) on three different IRMOFs: IRMOF-1, IRMOF-8 and IRMOF-10. The
84 IRMOF structure is made of Zn₄O tetranuclear clusters connected by rigid dicarboxylic linkers
85 to create a cubic framework, with square channels which are connected in the three

86 | dimensions [6]. These structures are very open and the crystal density is very low [25]. The
87 | linkers, terephthalic acid (IRMOF-1), 2,6-naphthalene dicarboxylic acid (IRMOF-8) and 4,4'-
88 | diphenyl dicarboxylic acid (IRMOF-10) confer the structured materials different open windows.
89 | The IRMOFs here chosen have no functional groups in the linkers, thus the resulting materials
90 | only differ on the sizes of the created cages. The inverse gas chromatography (IGC) was chosen
91 | as technique to study the interaction of organic compounds of selected families (*n*-alkanes,
92 | alkenes, cyclic, aromatic and chlorinated compounds) on these three IRMOFs. [This technique](#)
93 | [provides thermodynamic information about the adsorption, which can be used to estimate](#)
94 | [and compare the relative strengths of intermolecular forces between the adsorbent and](#)
95 | [different adsorbates, and to study the interactions between the adsorbate and the adsorbent](#)
96 | [\[26,27,28\]](#). IGC is a chromatographic technique that differs from the gas-solid chromatography
97 | in its goal: the characterization of the stationary phase, instead of the separation of solutes in
98 | the mobile phase. [Furthermore, IGC offers an alternative to the conventional gravimetric or](#)
99 | [volumetric methods for determining adsorption equilibrium isotherms, due to its simplicity,](#)
100 | [the shorter measurement time and a wider range of experimental possibilities.](#) ~~IGC~~
101 | ~~measurements can provide information on thermodynamic, surface energy, reaction kinetics,~~
102 | ~~and textural parameters (such as surface area and porosity).~~

103
104 | Thus, the scope of this work is to evaluate the interaction of selected organic compounds
105 | –representative of different families of VOCs– on three IRMOFs without functionalization of
106 | the organic linkers (IRMOF-1, IRMOF-8 and IRMOF-10) in order to evaluate adsorption
107 | behavior and correlate it to the morphologic structure of the network. IGC adsorption studies
108 | have been used for evaluating different thermodynamic parameters (adsorption capacity,
109 | adsorption enthalpy, entropy and free energy; as well as dispersive and specific contributions
110 | to these terms), useful for gaining further understanding on the adsorption features of these
111 | materials. To the best of our knowledge, there is only one work [24] dealing with the
112 | determination of thermodynamic properties (enthalpies of adsorption, free energies of
113 | adsorption and the dispersive and specific components of the surface free energy)
114 | systematically for different adsorbates on IRMOFs by IGC, specifically this work was devoted to
115 | the influence of synthesis procedure of IRMOF-1 on the adsorption of several organic
116 | compounds.

117

118

119 **2. Experimental**

120 **2.1. Synthesis of IRMOFs**

121 IRMOFs were synthesized at room temperature according to the method described in the
122 literature [2629], the main features of the procedures being summarised below.

123

124 For the synthesis of the IRMOF-1, 120 mmol of zinc acetate, $Zn(OAc)_2 \cdot 2H_2O$ (>98%, Sigma-
125 Aldrich), were dissolved in 774 mL of N,N'-dimethylformamide, DMF (99.8%, Panreac).
126 Likewise, 47.2 mmol of terephthalic acid (98%, Sigma-Aldrich) and 13 mL of triethylamine
127 (99%, Sigma Aldrich) were dissolved in 619 mL of DMF, where the molar ratio between
128 terephthalic acid and zinc acetate was 0.4. The zinc salt solution was added to the organic
129 solution with stirring during 15 min, and then the solution was stirred at 325 rpm for 2.5 h. The
130 precipitate was centrifuged at 6 500 rpm for 15 min to 293 K and immersed in 387 mL of DMF
131 overnight. Afterwards, it was centrifuged again and immersed in 542 mL of trichloromethane,
132 $CHCl_3$ (99%, Panreac). The solvent was exchanged 3 times over 7 days. The solution was
133 centrifuged and the white solid was dried in oven at 373 K for 48 h. The resulting solid was
134 activated at different temperatures (393, 473, 523 and 573 K) for 6 h, at a heating rate of 1
135 K/min under a helium atmosphere at a flow rate of 0.6 L/min. The IRMOF-1 was kept in a
136 desiccator to avoid its further contact with moisture and air.

137

138 IRMOF-8 and IRMOF-10 were synthesized following the same method and molar ratio as
139 the IRMOF-1, using 2,6-naphthalene dicarboxylic acid (95%, Sigma-Aldrich) and 4,4'-diphenyl
140 dicarboxylic acid (97%, Sigma-Aldrich) as organic compounds, respectively. The activation
141 temperature of materials was optimized following the BET surface area, in this way, 573 K was
142 chosen for IRMOF-1 and 8, whereas 523 K for IRMOF-10.

143

144 **2.2. Apparatus and procedure**

145 The crystallographic structures of the IRMOFs were determined by XRD using a Philips
146 X'Pert Pro powder diffractometer, working with the $Cu-K\alpha$ line ($\lambda = 0.154$ nm) in the range 2θ
147 between 5° and 20° at a scanning rate of $0.02^\circ/s$. The X-ray tube voltage and current were set
148 at 45 kV and 40 mA, respectively.

149

150 Specific surface area, pore diameter and volume were estimated by nitrogen adsorption
151 at 77 K in a Micromeritics ASAP 2020 surface area and porosity analyzer. The surface area (S_{BET})
152 was calculated according to the Brunauer-Emmett-Teller (BET) method, whereas the
153 micropore volume ($V_{\text{micropores}}$) was obtained using the Harkins and Jura t method. The average
154 pore diameter (D_p) and mesopore volume ($V_{\text{mesopores}}$), were determined from the desorption
155 branch using the Barrett-Joyner-Halenda (BJH) method.

156

157 The thermal decomposition of IRMOFs were characterised by thermogravimetric analysis
158 in a TG-DSC (Setaram, Sensys). A sample of material (20 mg) - and α -alumina as inert reference
159 material- was treated in Pt crucibles at a heating rate of 5 K/min from 298 to 973 K in N_2
160 atmosphere at a flow rate of 20 mL/min.

161

162 Adsorption measurements were carried out in a conventional gas chromatograph (Varian
163 model 3800) with a thermal conductivity detector (TCD). About 0.25 g of each IRMOF was
164 placed into a 25 cm length of Supelco Premium grade 304 stainless steel column ([about 4 cm](#)
165 [of IRMOF packed](#)), with passivated inner walls and inside diameter of 5.3 mm. Pyrex glass,
166 between 250-355 μm , was used as inert material to fill the column and at the ends of itself was
167 used silanized glass wool to prevent any loss of the adsorbent. The columns were stabilized in
168 the GC system at 573 K (IRMOF-1 and IRMOF-8) and at 523 K (IRMOF-10) overnight under a
169 helium flow rate of 30 mL/min.

170

171 Measurements were performed in the temperature range of 393 – 423 K. Helium
172 (99.999%, Praxair) was used as carrier gas, for all experiments, at a flow rate of 30 mL/min,
173 which was measured using a calibrated soap bubble flowmeter. [Samples injected consists of](#)
174 [0.1 \$\mu\text{L}\$ of adsorbate, in](#) order to satisfy the requirement of adsorption at infinite dilution,
175 [corresponding to zero coverage and GC linearity, the samples injected were](#) and 0.1 μL of
176 [adsorbate and the same amount of air, to meet the time out](#) in order to estimate the dead
177 [time of the column](#). The validity of [this the zero coverage](#) hypothesis was confirmed by the
178 symmetry of the elution peaks and by the constancy of the retention times measured over the
179 range of the sample sizes studied. The specific retention volume, V_g , in cm^3/g , was calculated
180 using the equation:

181

$$V_g = F j \frac{t_R - t_M}{m} \left(\frac{p_0 - p_w}{p_0} \right) \left(\frac{T}{T_{\text{meter}}} \right) \quad (1)$$

182

183

$$j = \frac{3}{2} \left[\frac{\left(\frac{p_i}{p_o}\right)^2 - 1}{\left(\frac{p_i}{p_o}\right)^3 - 1} \right] \quad (2)$$

184
185
186 where F is the volumetric flow rate of carrier gas, j the James-Martin compressibility factor, t_R
187 the retention time, t_M the retention time of a non-adsorbing marker (air), m the mass of the
188 adsorbent, p_o the outlet column pressure, p_w the vapour pressure of water at the flowmeter
189 temperature, T_{meter} the ambient temperature and p_i the inlet column pressure. The meaning of
190 the symbols is indicated in the list of symbols. For each measurement, the adsorbent
191 adsorbate was injected three times, obtaining reproducible results ($\pm 5\%$ retention volume).
192 Chromatographic measurements of a given compound (n-hexane) were randomly repeated
193 during the use of each column in order to ensure the stability of the material. The procedures
194 used for the calculation of adsorption parameters (capacities Henry constants, enthalpies, free
195 energies, entropies and the surface free energy, both the specific and the dispersive
196 components) from IGC experiments are described in detail in a previous work [2730].

197
198 The selected adsorbates, representative of different families of volatile organic
199 compounds are: *n*-pentane (99%, Panreac), *n*-hexane (99%, Sigma-Aldrich), *n*-heptane (99%,
200 Sigma-Aldrich), *n*-octane (99.5%, Sigma-Aldrich), 1-hexene (97%, Sigma-Aldrich), cyclohexane
201 (98%, Panreac), methylcyclohexane (99%, Fluka), benzene (99%, Panreac), toluene (99.5%,
202 Panreac), chlorocyclohexane (98%, Fluka), trichloroethylene and tetrachloroethylene (99%,
203 Panreac).

204 205 206 **3. Results and discussions**

207 **3.1. Textural and morphologic characterization of adsorbents**

208 XRD patterns of synthesized IRMOFs samples are shown in Fig. 1. For IRMOF-1, it is
209 observed that the main peaks at $2\theta = 6.5$ and 9.5° are dismissed in comparison to simulated
210 diffractograms [24]. The decrease in the size of the main peaks is related to the influence of
211 guest molecules in the structure [2831]. Likewise, a dominating peak at $2\theta = 8.7^\circ$ is observed,
212 being attributed this peak to the presence of a nonporous phase resulting from water induced
213 structural degradation [2932]. The IRMOF-8 shows two main peaks at $2\theta = 6.0$ and 8.5° ,
214 consistent with data observed in the literature [3033]. However, three small peaks at
215 $2\theta = 11.8$ - 13.3° are also observed, that could indicate the presence of lattice defects such as

216 | metal cluster in the pores or lattice interpenetration [3134]. For IRMOF-10, three peaks are
217 | observed: the main one at $2\theta = 6.4^\circ$, and two minor ones at $2\theta = 5.2$ and 10.4° , although the
218 | relative order of the intensities does not follow the trend reported for simulated diffractograms
219 | [3235]. This fact is also related, as in the case of IRMOF-1, -to the presence of guest molecules
220 | in the structure.

221

222 | The morphology of these structures was determined by nitrogen sorption analysis at 77 K,
223 | Fig. 2 showing the adsorption-desorption isotherms. All of materials characterized clearly
224 | corresponded to type I (microporous solids), according to the IUPAC classification. The textural
225 | properties of the samples are summarized in Table 1. The BET surface areas of IRMOFs studied
226 | decrease from 1 to 10. For IRMOF-1, the BET area is similar to that reported in the literature
227 | for these materials: $2900 \text{ m}^2/\text{g}$ by Eddaoudi et al. [3336] and $3362 \text{ m}^2/\text{g}$ by Rowell et al. [10].
228 | Also similar values have been found for IRMOF-8, Wang et al. [3437] reporting an area of
229 | $1343 \text{ m}^2/\text{g}$. It should be pointed out that in all cases the IRMOFs were synthesised by the
230 | solvothermal method, and there are not evidences about the decomposition of the material
231 | during the chromatographic experiments. At this point, samples prepared through microwave-
232 | assisted methods exhibit higher surface areas, but these structures are not stable at the
233 | operation conditions. However, in good agreement with the XRD findings, the greatest
234 | differences are observed for IRMOF-10: the surface area ($265 \text{ m}^2/\text{g}$) of this material is one
235 | order of magnitude lower than the BET area reported by Bae et al. [3538], although in this case
236 | the surface area was not experimental but calculated using simple geometrical techniques.
237 | Pore volume, both microporous and mesoporous, and pore diameter are consistent with the
238 | surface area data.

239

240 | The thermal evolution of the IRMOFs is a key point because these materials will be used
241 | as adsorbents and desorption will be carried out by increasing temperatures. The typical
242 | thermogravimetric-differential thermogravimetric (TG-DTG) profile of the IRMOFs treatment is
243 | shown in Fig. 3. Thermal behavior is nearly the same in all cases. A first region, associated to a
244 | DTG peak around 350 K, is observed, attributed to N,N'-dimethylformamide loss [3639]. A
245 | sharp weight loss occurs from 650 K, indicating the collapse of the structure. This phenomenon
246 | was reported to occur between 573 and 773 K [3639,3740]. According to these results, IRMOFs
247 | structures seem to be an interesting alternative to more conventional adsorbents, since
248 | thermal treatment produces the selective decomposition of the oxygenated groups of
249 | activated carbons, even at lower temperatures [3841], and in the case of zeolites, the
250 | thermolysis of the template could begin at 573 K [3942].

251

252

253 **3.2. Adsorption parameters**

254 According to the procedure outlined in the previous papers [2730,4043], adsorption
255 isotherms were determined in the region of infinite dilution, the so-called Henry's law region,
256 using the elution by characteristic point (ECP) method, neglecting the 10 % lower part of the
257 elution peaks, and correcting them by the Betchold method. Henry's constant values, at 423 K
258 (<1% of variation between successive measurements), for an *n*-alkane compound (*n*-hexane),
259 an alkene (1-hexene), cyclic (cyclohexane and methylcyclohexane), aromatic (benzene and
260 toluene) and chlorinated compounds (trichloroethylene and tetrachloroethylene), are shown
261 in Fig. 4. These constants are measured at the linear portion of the isotherm, where the
262 interactions between adsorbed molecules can be neglected. For all the compounds, the
263 Henry's constant increases in the order: IRMOF-1 < IRMOF-8 < IRMOF-10. Luebbers et al. [24],
264 in a study about the adsorption of VOCs on three different IRMOF-1 by IGC, reported also
265 higher values of the Henry's constant for materials with the lowest surface area, attributing
266 this result to the structural degradation of the sample, due to changes in pore geometry,
267 increasing the surface area accessible for nitrogen molecules but not the available for the
268 adsorption of larger VOCs. However, these authors are comparing the same IRMOF, prepared
269 under different conditions. The same explanation could be plausible here, and consistent with
270 XRD data. Furthermore, the aromatic compounds, as well as trichloroethylene and
271 tetrachloroethylene are, in general terms, the compounds with the highest adsorption
272 capacity, whereas the linear and cyclic compounds exhibit markedly lower values for the
273 Henry's constant. These data suggest that the π -bonds are determinant in the capacity of
274 adsorption, and more important than the molecular sizes or the dipolar moment reported for
275 carbon materials as it was already shown for the adsorption of hydrocarbons on ZIF-8 [4144].

276

277 A positive linear relationship between the Henry's constant for the *n*-alkanes and their
278 molecular cross-sectional area (i.e. the area of the projection of a molecule where a spherical
279 molecular shape in a hexagonal close-packed configuration is accepted [452]) was observed,
280 Fig. 5. This phenomenon, which is not observed for the other compounds, implies that the
281 interaction between the surface of IRMOFs and the adsorbates increases with the size of the
282 molecule. Furthermore, it is notorious that whereas differences are scarce for IRMOF-8 and
283 IRMOF-10 for *n*-pentane to *n*-heptane, larger differences are observed for *n*-octane, and also
284 lower slope is observed for IRMOF-1. This behavior can be understood taking into account that

285 | ~~whereas~~ two of the three dimensions of *n*-alkanes are very similar (~~molecular x-axis one of~~
286 | ~~them~~ is equal the same for all *n*-alkanes and the variation of the other one between *n*-pentane
287 | and *n*-octane is about just 0.015 Å ~~between *n*-pentane and *n*-octane for y axis was measured~~),
288 | whereas the third one axis presents variations from ~~the~~ 9.1 Å for *n*-pentane to 12.8 Å for *n*-
289 | octane [436]. Taking into account the pore openings of Table 1, *n*-pentane is the only *n*-alkane
290 | which is not limited by the diameter of the entrance cavity in any IRMOF, thus this justifies the
291 | lowest slope for IRMOF-1. Concerning the different behavior of *n*-octane for IRMOF-8 and
292 | IRMOF-10, it is remarked that it could still cross freely the IRMOF-10 pores but not the IRMOF-
293 | 8.

294
295 | The strength of the interaction of each compound with the surface of the adsorbent is
296 | represented by the enthalpy of adsorption, $-\Delta H_{ads}$, given by Eq. (3):

$$\Delta H_{ads} = -R \frac{\partial(\ln V_g)}{\partial\left(\frac{1}{T}\right)} \quad (3)$$

298
299
300 | Adsorption enthalpies were achieved from the slope of plots of $\ln V_g$ vs. $1/T$, where this
301 | linear dependence implies a constant value of the enthalpy of adsorption in the range of
302 | studied temperatures (393 - 423 K). Results of adsorption enthalpies are showed in Table 2,
303 | whereas the parent plots, recorded at four different temperatures are provided as
304 | Supplementary Information. The heats of liquefaction (ΔH_{liq}) [474] are also reported in this
305 | table, ~~observing that the d~~ differential heats of adsorption over the three IRMOFs are higher
306 | than the heats of liquefaction, thus adsorbate-adsorbent interactions are stronger than
307 | adsorbate-adsorbate ones. In general, the strength of the adsorption increases with the size of
308 | the cage of IRMOF, in agreement with Henry's constants. This fact could seem contradictory,
309 | since usually at a given loading, the adsorbate-framework strength of interaction increases
310 | with the lower pore diameter as the molecules are forced to be closer together in the small
311 | pores. At this point, it is necessary to point out that the surface area of the IRMOFs under
312 | study decreases with the increasing cavity size (Table 1), due to the presence of a nonporous
313 | phase. This hypothesis is confirmed by comparison of the measured enthalpies of adsorption
314 | for IRMOF-1 with the equivalents reported by Luebbers et al. [24] over three different samples
315 | of IRMOFs-1. For all common adsorbates analysed, Luebbers et al. [24] reported values of
316 | enthalpy of adsorption higher than the reported in this work, which is justified attending to the
317 | lower S_{BET} reported: 1161, 781 and 208 m^2/g . Likewise, since the adsorption of organic
318 | molecules is considered, they would have higher affinity for organic compounds, thus this also

319 justifies that the strength to adsorption increases with the number of carbon atoms in the
 320 linker molecule: $-\Delta H_{\text{ads,IRMOF-1}} < -\Delta H_{\text{ads,IRMOF-8}} < -\Delta H_{\text{ads,IRMOF-10}}$. This appreciation is in good
 321 agreement with molecular simulations of *n*-butane adsorption on IRMOFs [25], where it was
 322 observed that *n*-butane isosteric heat of adsorption was higher for IRMOF-14 than for IRMOF-
 323 8. Comparing the enthalpies of adsorption of IRMOFs with more conventional adsorbents such
 324 as alumina, zeolites or activated carbons [4043], it is observed that differences among
 325 different materials are even lower than between the three IRMOFs here studied; and, in all
 326 cases higher than for non microporous carbons such as carbon nanotubes, carbon nanofibers
 327 or high-surface-area graphites [4048].

328

329 From chromatographic data, the standard free energy of adsorption at infinite dilution,
 330 $-\Delta G_{\text{ads}}(\text{kJ/mol})$, and the entropy of adsorption, $-\Delta S_{\text{ads}}(\text{J/mol K})$, were also calculated according
 331 to the procedure outlined in a previous work [485]. Briefly, the standard free energy of
 332 adsorption at infinite dilution, $-\Delta G_{\text{ads}}(\text{kJ/mol})$, can be expressed by Eq. (4):

$$333 \quad \Delta G_{\text{ads}} = -RT \ln \left[\frac{p_0 V_g}{\pi_0 A} \right] \quad (4)$$

334

335 Where A is the specific surface area of the adsorbent, and π_0 is the spreading pressure of
 336 the adsorbed gas in the De Boer standard state, which was taken as 338 $\mu\text{N/m}$. The other
 337 symbols were already indicated in the text.

338 ~~The meaning of the symbols is indicated in the list of symbols.~~ Subsequently, the entropy
 339 of adsorption is calculated straightforwardly according to Eq. (5):

$$340 \quad \Delta S = \frac{\Delta H - \Delta G}{T} \quad (5)$$

341

342 Results obtained are summarized in Table 2. The trend observed for all the IRMOFs was
 343 consistent over the whole temperature interval studied, although being only shown the data
 344 obtained at 423 K for simplicity. Fig.6 shows the existence of a so-called “thermodynamic
 345 compensation effect”, i.e., a linear dependence of ΔS on ΔH . This effect for *n*-alkanes indicates
 346 that the stronger adsorption of longer *n*-alkanes is accompanied by a greater loss of mobility of
 347 the molecules (this means stronger interaction between the molecule and the surface). This
 348 type of plot allows highlighting differences in adsorbate–adsorbent interactions. A good fit of
 349 the compensation effect data to a straight line indicates the non specific nature of the
 350 adsorbate–adsorbent interactions. In the case of Fig. 6, just one straight line is depicted. Thus,

351 the lattice defects or the differences on the organic linkers do not affect the interaction of *n*-
 352 alkanes on these IRMOFs, suggesting that the surface of the studied materials is chemically
 353 analogous. In fact, as the organic linkers of the studied IRMOFs have not any functionality, the
 354 nature of the interaction does not vary with the size of the cage.

355

356 The interaction of *n*-alkanes with the surface has been also studied attending to the
 357 dispersive component of the surface free energy of the adsorbent. The dispersive component,
 358 γ_S^D , is attributed to London forces and it is unspecific for all molecules. Comparing to the
 359 enthalpy of adsorption, this parameter is slightly more sensitive to surface changes. The
 360 formula of Dorris and Gray has been used to calculate the values of this parameter [4496]:

361

$$362 \quad \gamma_S^D = \frac{1}{4} \frac{\Delta G_{CH_2}^2}{\gamma_{CH_2} N^2 a_{CH_2}^2} \quad (6)$$

363

364

365 where ΔG_{CH_2} is the difference between the free energy of adsorption of two *n*-alkanes with
 366 succeeding values of carbon atoms, N is the Avogadro number, a_{CH_2} is the area occupied by a -
 367 CH₂ group (0.06 nm²), and γ_{CH_2} (mJ/m²) is the surface tension of a surface consisting of CH₂
 368 groups, which is a function of temperature in °C:

369 ~~The meaning of the symbols is indicated in the list of symbols. The surface tension of a surface~~
 370 ~~consisting of CH₂ groups, γ_{CH_2} (mJ/m²), is a function of temperature in °C:~~

371

$$372 \quad \gamma_{CH_2} = 35.6 + 0.058 (20 - T) \quad (7)$$

373

374 Values of the dispersive component for the range of temperature studied are shown in
 375 Fig.7. The values of the dispersive component are very similar for the three tested adsorbents,
 376 indicating that the nature of the interaction is very similar as it was previously deduced from
 377 the thermodynamic compensation effect. In any case, it may be noteworthy that IRMOF-1
 378 exhibits values of γ_S^D slightly higher than the others IRMOFs. This difference was attributed to
 379 the increase in the interaction potential in the smallest pores. In fact, according to the textural
 380 characterization, due to the structural damage, IRMOF-1 has the lowest pore diameter and the
 381 highest surface area. In all cases, the dispersive component of the surface free energy
 382 decreases with the temperature, due to the entropic contribution to the surface energy. This
 383 difference is slightly more marked for IRMOF-10, in agreement with the highest values of the

384 entropy. Comparing the values of the γ_S^D here reported with those of the literature, they are
385 very similar to those obtained by Luebbers et al. [24] for IRMOF-1, and much lower than those
386 obtained, also by IGC, for microporous materials such as zeolites or activated carbons [4043].

387
388 Adsorption of *n*-alkanes takes place through dispersive interactions, yielding information
389 related to carbon structure, polar probes are needed to determine the acid–base character of
390 the surfaces. The adsorption of these molecules on the stationary phase involves, in addition
391 to the dispersive interactions, specific contributions. One of the most useful methods is the
392 “parameter of specific interaction”, I^{sp} , which is determined from the difference in free energy
393 of adsorption between a polar solute and the real or hypothetical *n*-alkane with the same
394 surface area [4507]:

$$I^{sp} = \frac{\Delta(\Delta G)}{Na} = \frac{\Delta G_{ads}^S}{Na} \quad (8)$$

395
396
397 Where a is the probe surface area. Although this parameter has several sources of errors, it is
398 satisfactory for those adsorbents without functional groups, and with values of γ_S^D lower than
399 100 mJ/m² [5148]. The specific interaction parameters for the IRMOFs as well as the area of
400 the projection of the molecule probe (nm²), the dipolar moment (D) and the polarizability
401 deformation (Cm² V⁻¹) of the molecules are summarized in Fig. 8. It is worth noting that
402 cyclohexane and methylcyclohexane show the lowest values of the I^{sp} . Contrary, aromatic
403 compounds and trichloroethylene as well as tetrachloroethylene exhibit the largest specific
404 interaction. As can be seen from Fig. 8, this behavior cannot be exclusively explained attending
405 to the surface area of the molecules, thus, add to the structure effects detected by the *n*-
406 alkanes adsorption dependence on the cavity size, other effects are also present. It is also
407 remarkable, that the dipolar moment (a parameter that could be expected to be relevant in
408 the specific interaction) is especially relevant for chlorocyclohexane, compound with a quite
409 moderate specific interaction. Finally, the molecular polarizability of the different polar
410 adsorbates could be, with some exceptions, an indicative of the specificity of this interaction.
411 Thus, in order to assess the degree of importance of each of these parameters on the
412 specificity of the interaction of these compounds, all of them have been adjusted according to
413 the following expression:

$$I^{sp} = \alpha \cdot \text{surface area of molecule} + \beta \cdot \text{dipolar moment} + \chi \cdot \text{polarizability} \quad (9)$$

415

416 The fitting parameters (α, β, χ) were obtained for three different families of compounds,
417 for the three IRMOFs under study. The goodness of the fit is shown in Fig. 9. It was found that
418 for cyclohexane and methylcyclohexane, the most important parameters were the dipolar
419 moment of the adsorbates ($\beta=14.3$), and in lower extent, their polarizability ($\chi=1.6$). However,
420 for the aromatic and the chlorinated compounds, the polarizability ($\chi=4.1$ and 3.2 ,
421 respectively) of the molecules seems to be the most important parameter ($\alpha \approx \beta \approx 0$).
422 Furthermore, it is remarkable that the compounds with π - π bonds (trichloroethylene,
423 tetrachloroethylene and aromatic compounds) are those with the largest values of I^{sp} , thus the
424 specific interactions between the π -electron rich regions of the organic linkers and the double
425 bonds of the molecules enhanced the adsorption. This observation is in agreement with
426 molecular simulations of methane and butane on IRMOFs, showing that interaction energy
427 was stronger as the number of carbon atoms in the linker molecule increases and the cavity
428 size decreases [25].

429

430

431

432 **4. Conclusions**

433 Inverse gas chromatography has been used as technique to determine the adsorption
434 properties of several organic compounds on three different IRMOFs, with cubic structure and
435 without functionalities on the organic linkers: IRMOF-1, IRMOF-8 and IRMOF-10. It is shown
436 that the capacity of adsorption at infinite dilution and the enthalpy of adsorption increase with
437 the cavity diameter of the structures. For *n*-alkanes it is deduced a size dependence related to
438 the pore opening of the IRMOFs. As general trend, it is observed that the strength of the
439 interaction increases in the order IRMOF-1 < IRMOF-8 < IRMOF-10 because of two
440 complementary effects: the presence of the lattice defects and the increase in the number of
441 carbon atoms of the organic linkers. Likewise, from the thermodynamic compensation effect
442 and the dispersive component of the surface free energy is deduced that the *n*-alkanes present
443 the same centres of adsorption on the three IRMOFs. Concerning the specific interaction
444 component, it was observed that the presence of π -electron rich zones (aromatic rings or
445 double bonds) enhanced the specificity of the interaction by the favoured interaction with the
446 aromatic rings of the organic linker molecules. Therefore, the specificity of the interactions is
447 more related to the chemistry of the organic linkers than the structure of the IRMOFs.

448

449

450 Acknowledgements

451 This work was supported by the Research Fund for Coal and Steel of the European Union
452 (contract UE-10-RFCR-CT-2010-00004) and the Spanish Government (contract CTQ2011-29272-
453 C04-02). I. Gutiérrez thanks the Government of the Principality of Asturias for a Ph. D.
454 fellowship (Severo Ochoa Program).

455 Nomenclature

456 *Latin symbols*

457 σ ————— probe surface area
458 A ————— surface area of the adsorbent
459 a_{CH_2} ————— area occupied by a CH_2 group (0.06 nm^2)
460 F ————— volumetric flow rate of carrier gas
461 I^{sp} ————— specific interaction parameter
462 j ————— James-Martin compressibility factor
463 m ————— mass of the adsorbent
464 N ————— is the Avogadro number
465 p_i ————— inlet column pressure.
466 p_o ————— outlet column pressure
467 p_w ————— vapour pressure of water at the flowmeter temperature
468 t_M ————— the retention time of a non-adsorbing marker (air)
469 t_R ————— retention time
470 R ————— ideal gas constant
471 T ————— operation temperature
472 T_{meter} ————— ambient temperature
473 V_g ————— specific retention volume

474 *Greek symbols*

475 ΔG_{ads} ————— free energy of adsorption
476 ΔG_{CH_2} ————— difference between the free energy of adsorption of two n alkanes with
477 succeeding values of carbon atoms
478 ΔH_{ads} ————— enthalpy of adsorption
479 ΔH_{liq} ————— heat of liquefaction
480 ΔS_{ads} ————— entropy of adsorption
481 γ_{CH_2} ————— surface tension of a surface consisting of CH_2 groups
482 γ_S^D ————— dispersive component of the surface free energy of the adsorbent
483 π_o ————— spreading pressure of the adsorbed gas in the De Boer standard state, 338
484 $\mu\text{N/m}$

486

487 **References**

- 488 [1] M. Xue, Y. Liu, R. M. Schaffino, S.C. Xiang, X. J. Zhao, G. S. Zhu, S. L. Qiu, B. L. Chen, *Inorg.*
489 *Chem.* 48 (2009) 4649.
- 490 [2] H. Li, M. Eddaoudi, M. O'Keeffe, O. M. Yaghi, *Nature* 402 (1999) 276.
- 491 [3] O. M. Yaghi, M. O'Keeffe, N. W. Ockwig, H. K. Chae, M. Eddaoudi, J. Kim, *Nature*
492 423(2003) 705.
- 493 [4] N. L. Rosi, J. Kim, M. Eddaoudi, B. L. Chen, M. O'Keeffe, O. M. Yaghi, *J. Am. Chem. Soc.* 127
494 (2005) 1504.
- 495 [5] J. L. Rowsell, E. C. Spencer, J. Eckert, J. A. K. Howard, O. M. Yaghi, *Science* 309 (2005)
496 1350.
- 497 [6] M. Eddaoudi, J. Kim, N. Rosi, D. Vodak, J. Wachter, M. O'Keeffe, O. M. Yaghi, *Science* 295
498 (2002) 469.
- 499 [7] G. Férey, C. Mellot-Draznieks, C. Serre, F. Millange, *Acc. Chem. Res.* 38 (2005) 217.
- 500 [8] M. J. Rosseinsky, *Microporous Mesoporous Mater.* 73 (2004) 15.
- 501 [9] J. L. C. Rowsell, O. M. Yaghi, *Angew. Chem. Int. Ed.* 44 (2005) 4670.
- 502 [10] J. L. C. Rowsell, A. R. Millward, K. S. Park, O. M. Yaghi, *J. Am. Chem. Soc.* 126 (2004) 5666.
- 503 [11] B. Panella, M. Hirscher, H. Pütter, U. Müller, *Adv. Funct. Mater.* 16 (2006) 520.
- 504 [12] K. M. Thomas, *Catal. Today* 120 (2007) 389.
- 505 [13] S. Kitagawa, R. Kitaura, S.-I. Noro, *Angew. Chem. Int. Ed. Engl.* 43 (2004) 2334.
- 506 [14] M. P. Suh, Y. E. Cheon, E. Y. Lee, *Coord. Chem. Rev.* 252 (2008) 1007.
- 507 [15] U. Mueller, M. Schubert, F. Teich, H. Puetter, K. Schierle-Arndt, J. Pastre, *J. Mater. Chem.*
508 16 (2006) 626.
- 509 [16] D. J. Collins, H. Zhou, *J. Mater. Chem.* 17 (2007) 3154.
- 510 [17] F. X. Llabrés i Xamena, A. Corma, H. García, *J. Phys. Chem. C* 111 (2007) 80.
- 511 [18] L. Alaerts, C. E. A. Kirschhock, M. Maes, M. A. van der Veen, V. Finsky, A. Depla, J. A.
512 Martens, G. V. Baron, P. A. Jacobs, J. F. M. Denayer, D. E. De Vos, *Angew. Chem. Int. Ed.* 46
513 (2007) 4293.
- 514 [19] P. S. Bárcia, F. Zapata, J. A. C. Silva, A. E. Rodrigues, B. Chen, *J. Phys. Chem. B* 111 (2007)
515 6101.
- 516 [20] D. Farrusseng, C. Daniel, C. Gaudillère, U. Ravon, Y. Schuurman, C. Mirodatos, D.
517 Dubbeldam, H. Frost, R. Q. Snurr, *Langmuir* 25 (2009) 7383.
- 518 [21] K. Yang, Q. Sun, F. Xue, D. Lin, *J. Hazard. Mater.* 195 (2011) 124.
- 519 [22] J. W. Jiang, S. I. Sandler, *Langmuir* 22 (2006) 5702.

520 [23] M. P. M. Nicolau, P. S. Barcia, J. M. Gallegos, J. A. C. Silva, A. E. Rodrigues, B. Chen, J.
521 Phys. Chem. C 113 (2009) 13173.

522 [24] M. T. Luebbers, T. Wu, L. Shen, R. I. Masel, Langmuir 26 (2010) 11319.

523 [25] T. Duren, R. Q. Snurr, J. Phys. Chem. B 108 (2004) 15703.

524 [\[26\] A. van Asten, N. van Veenendaal, S. Koster, J. Chromatogr. A 888 \(2000\) 175.](#)

525 [\[27\] F. Thielmann, J. Chromatogr. A 1037 \(2004\) 115.](#)

526 [\[28\] A. Voelkel, B. Strzemiecka, K. Adamska, K. Milczewska, J. Chromatogr. A 1216 \(2009\)](#)
527 [1551.](#)

528 ~~[26]~~~~[29]~~ D.J. Tranchemontagne, J.R. Hunt, O.M. Yaghi, Tetrahedron 64 (2008) 8553.

529 ~~[27]~~~~[30]~~ E. Dıaz, S. Ordonez, A. Vega, J. Coca, Microporous_Mesoporous Mater. 70
530 (2004) 109.

531 ~~[28]~~~~[31]~~ J. Hafizovic, M. Bjorgen, U. Olsbye, P. D. C. Dietzel, S. Bordiga, C. Prestipino, C.
532 Lamberti, K. P. Lillerud, J. Am. Chem. Soc. 129 (2007) 3613.

533 ~~[29]~~~~[32]~~ S.S. Kaye, A. Dailly, O.M. Yaghi, J.R. Long, J. Am. Chem. Soc. 129 (2007) 14176.

534 ~~[30]~~~~[33]~~ O. M. Yaghi, M. Eddaoudi, H. Li, J. Kim, N. Rosi, United States Patent 6930193
535 B2 (2005).

536 ~~[31]~~~~[34]~~ C-Y. Wang, C-S. Tsao, M-S. Yu, P-Y. Liao, T-Y. Chung, H-C. Wu, M. A. Miller, Y-R.
537 Tzeng, J. Alloys Comp. 492 (2010) 88.

538 ~~[32]~~~~[35]~~ O.K. Farha, K.L. Mulfort, A.M. Thorsness, J.T. Hupp, J. Am. Chem. Soc. 130
539 (2008) 8598.

540 ~~[33]~~~~[36]~~ M. Eddaoudi, D.B. Moler, H. Li, B. Chen, T. M. Reineke, M. O'Keeffe, O.M. Yaghi,
541 Acc. Chem. Res. 34 (2001) 319.

542 ~~[34]~~~~[37]~~ L. Wang, N. R. Stuckert, H. Chen, R. T. Yang, J. Phys. Chem. C 115 (2011) 4793.

543 ~~[35]~~~~[38]~~ Y-S. Bae, R. Q. Snurr, Microporous Mesoporous Mater. 132 (2010) 300.

544 ~~[36]~~~~[39]~~ J. Li, S. Cheng, Q. Zhao, P. Long, J. Dong, Int. J. Hydrogen Energy 34(2009)
545 1377.

546 ~~[37]~~~~[40]~~ J.L.C. Rowsell, O.M. Yaghi, Microporous_Mesoporous Mater. 73 (2004) 3.

547 ~~[38]~~~~[41]~~ F. Rodrıguez-Reinoso, M. Molina-Sabio, Adv. Coll. Interf. Sci. 76 (1998) 271.

548 ~~[39]~~~~[42]~~ M.A. Ali, B. Bridson, W.J. Thomas, Appl. Catal. A 252 (2003) 149.

549 ~~[40]~~~~[43]~~ E. Dıaz, S. Ordonez, A. Vega, J. Coca, ~~J. Microporous Mesoporous Mater. J.~~
550 [Chromatogr. A 1049 \(2004\) 139-82 \(2005\) 173](#)

551 [\[44\] M.T. Luebbers, T. Wu, L. Shen, R.I. Masel, Langmuir 26 \(2010\) 15625.](#)

552 [\[45\] P.N. Jacob, J.C. Berg, Langmuir, 10 \(1994\) 3086.](#)

553 [\[46\] C.E. Webster, R.S. Drago, M.C. Zerner, J. Am. Chem. Soc. 120 \(1998\) 5509.](#)

554 [\[47\] D. R. Lide, CRC Handbook of Chemistry and Physics, 80th ed., 1999-2000.](#)

- 555 | [\[48\] M. R. Cuervo, E. Asedegbega-Nieto, E. Díaz, A. Vega, S. Ordóñez, E. Castillejos-López, I.](#)
556 | [Rodríguez-Ramos, J. Chromatogr. A 1188 \(2008\) 264.](#)
- 557 | [\[49\] G. M. Dorris, D. G. Gray, J. Colloid Interface Sci. 77 \(1980\) 353.](#)
- 558 | [\[50\] J. Xie, Q. Zhang, K. T. Chuang, J. Catal. 191 \(2000\) 86.](#)
- 559 | [\[51\] J.B. Donnet, S.J. Park, H. Balard, Chromatographia 31 \(1991\) 434.](#)
- 560 |
- 561 |

562
563
564
565
566
567

Table 1. Textural properties of IRMOFs studied in this work.

IRMOF	S_{BET} m²/g	V_{micropores} cm³/g	V_{mesopores} cm³/g	D_p Å	Pore opening Å [25]
IRMOF-1	3046	1.103	0.115	24.9	10.9
IRMOF-8	1362	0.545	0.041	41.8	12.5
IRMOF-10	265	0.106	0.023	132.6	16.7

568
569
570
571
572

Table 2. Enthalpies of adsorption, standard free energies, entropies of adsorption and enthalpies of liquefaction of all adsorbates over the studied IRMOFs (free energies and entropies at 423 K).

Adsorbate	$-\Delta H_{\text{liq}}$ (kJ/mol)	$-\Delta H_{\text{ads}}$ (kJ/mol)			$-\Delta G_{\text{ads}}$ (kJ/mol)			$-\Delta S_{\text{ads}}$ (J/mol K)		
		IRMOF-1	IRMOF-8	IRMOF-10	IRMOF-1	IRMOF-8	IRMOF-10	IRMOF-1	IRMOF-8	IRMOF-10
<i>n</i> -Pentane	26.4	31.5	38.0	46.2	5.9	9.9	11.3	60.5	66.5	82.3
<i>n</i> -Hexane	31.6	34.1	49.2	50.8	8.6	14.1	12.8	60.5	83.0	89.6
<i>n</i> -Heptane	36.6	41.1	57.0	58.7	11.8	18.2	17.1	69.2	91.8	98.3
<i>n</i> -Octane	41.5	51.9	68.0	66.7	14.9	21.0	20.3	87.4	111.2	109.5
1-Hexene	30.6	32.7	45.7	41.1	8.5	14.2	13.3	57.3	74.5	65.9
Cyclohexane	33.0	34.1	35.9	37.6	8.0	13.7	10.3	61.9	52.5	64.4
Methylcyclohexane	35.4	38.2	48.0	47.5	10.2	16.7	12.2	66.2	74.0	83.4
Benzene	33.8	35.1	43.9	52.3	7.2	13.8	14.3	66.0	71.2	89.9
Toluene	38.0	42.1	59.6	64.3	9.9	18.3	19.5	76.0	97.5	105.7
Chlorocyclohexane	42.7	48.4	64.8	56.9	12.2	18.7	15.6	85.7	109.0	97.6
Trichloroethylene	34.5	41.3	52.9	58.0	7.9	14.9	15.9	79.0	89.8	99.7
Tetrachloroethylene	39.7	48.5	57.3	53.0	10.5	19.7	17.8	90.0	89.0	83.3

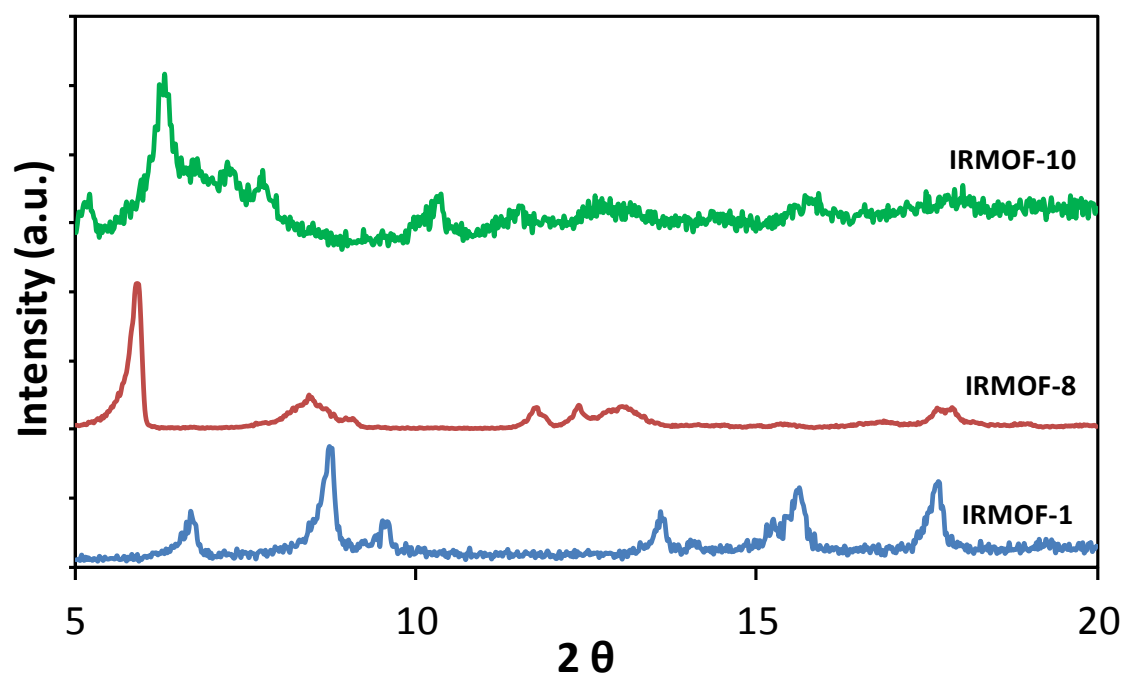


Figure 1.

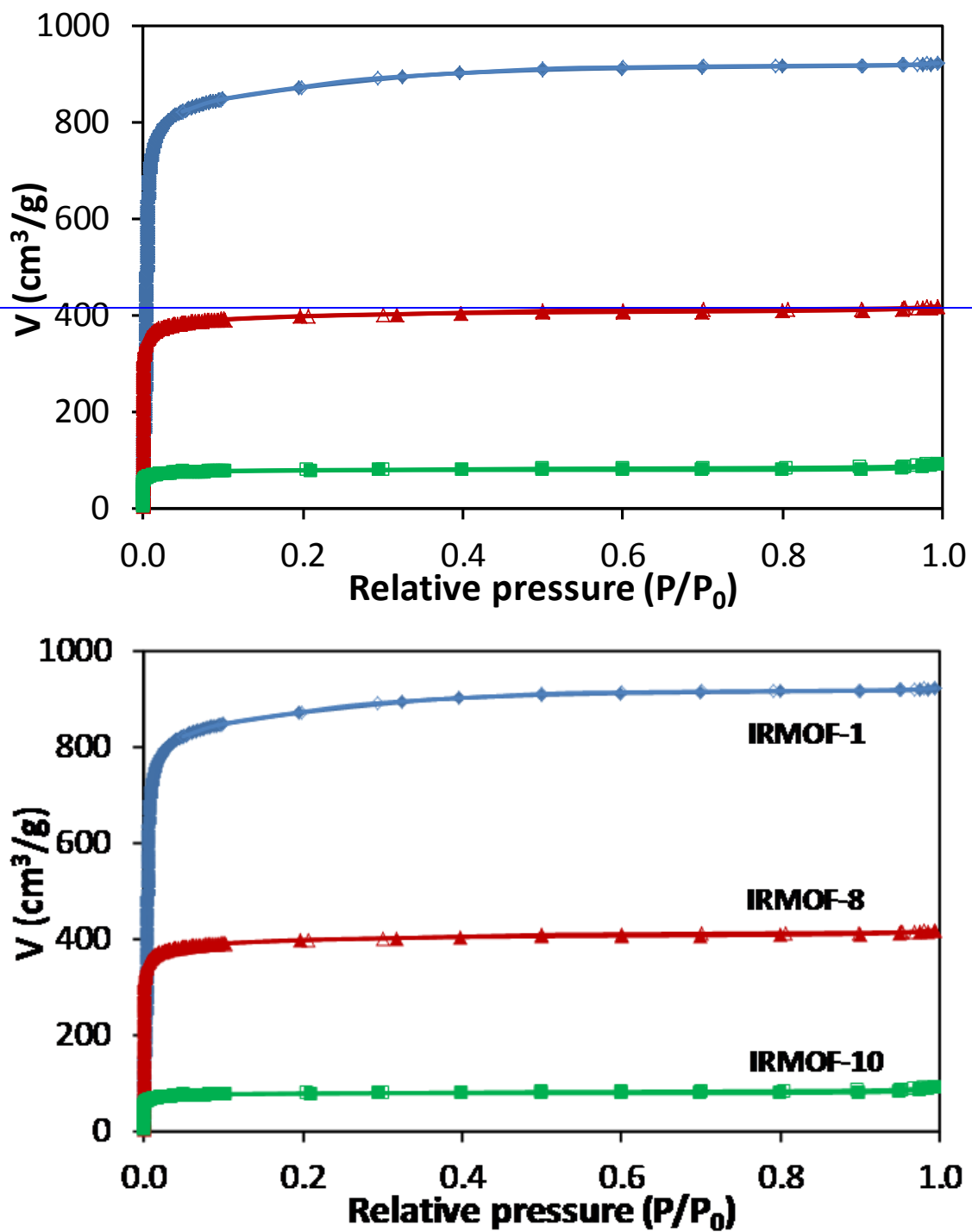
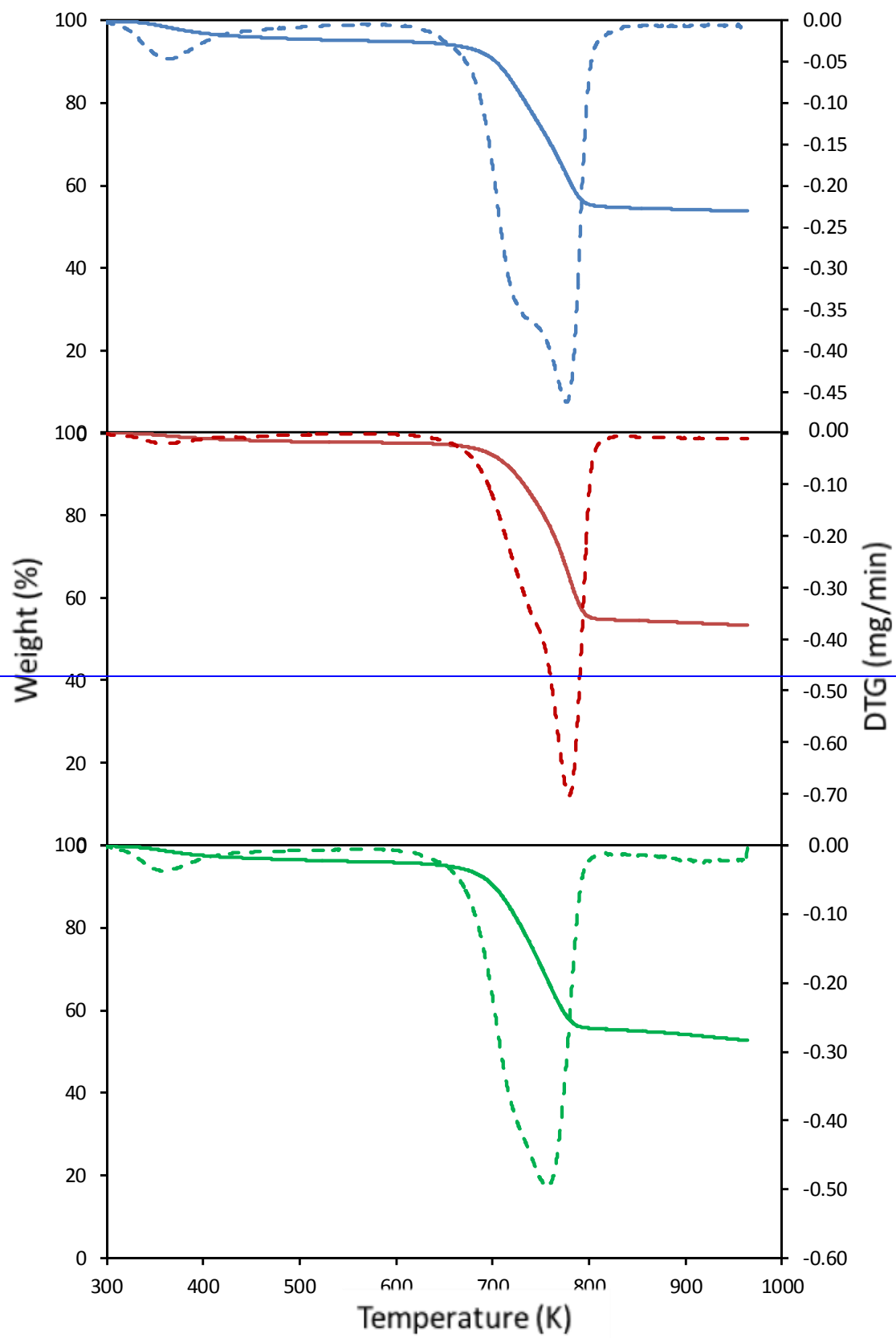


Figure 2.



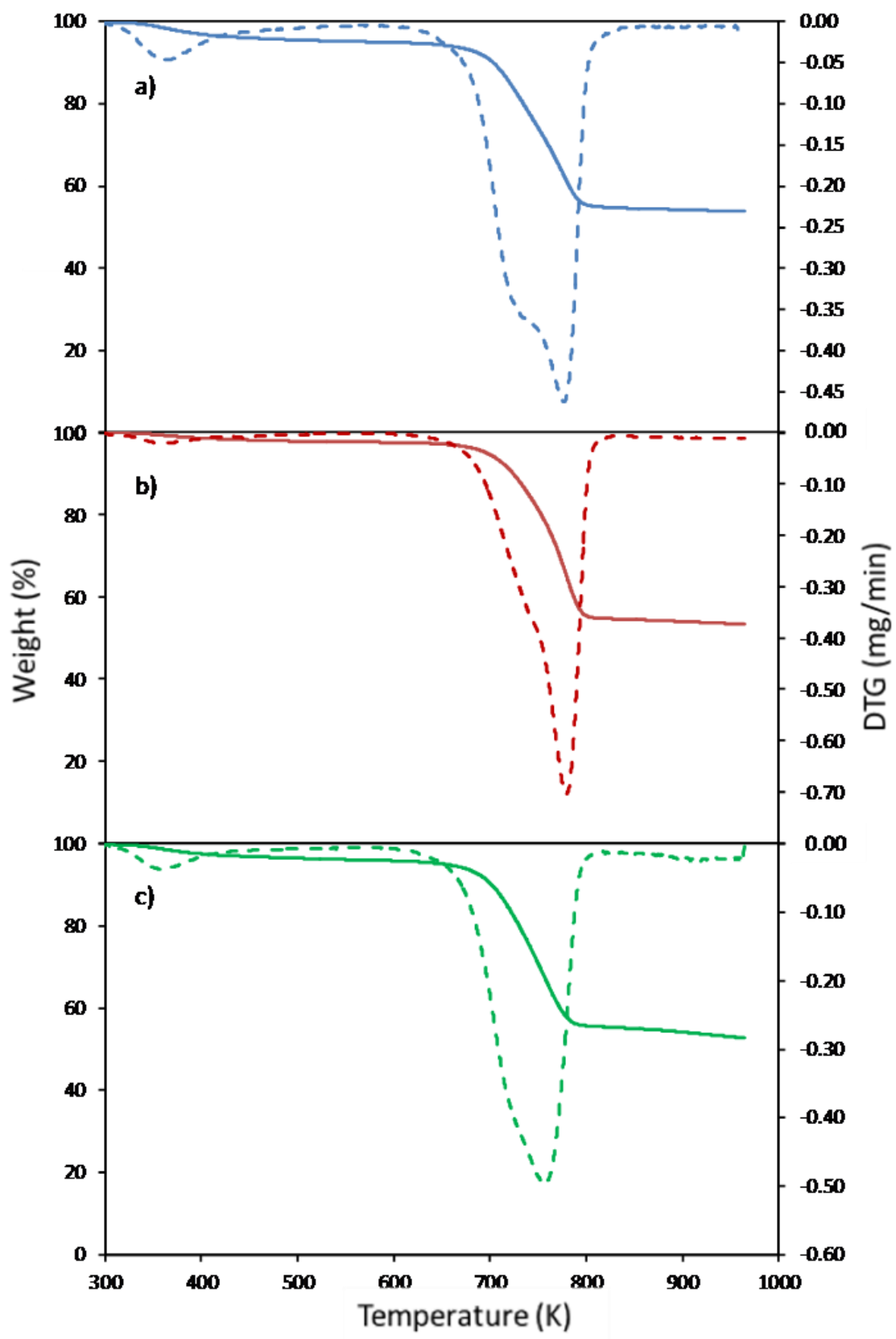
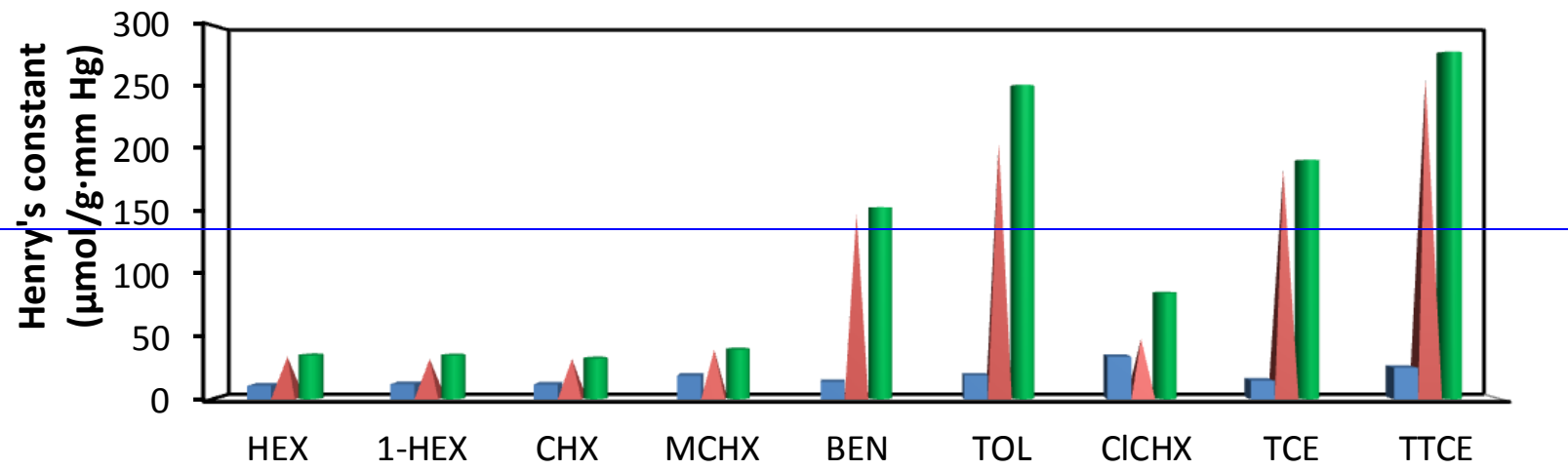


Figure 3.



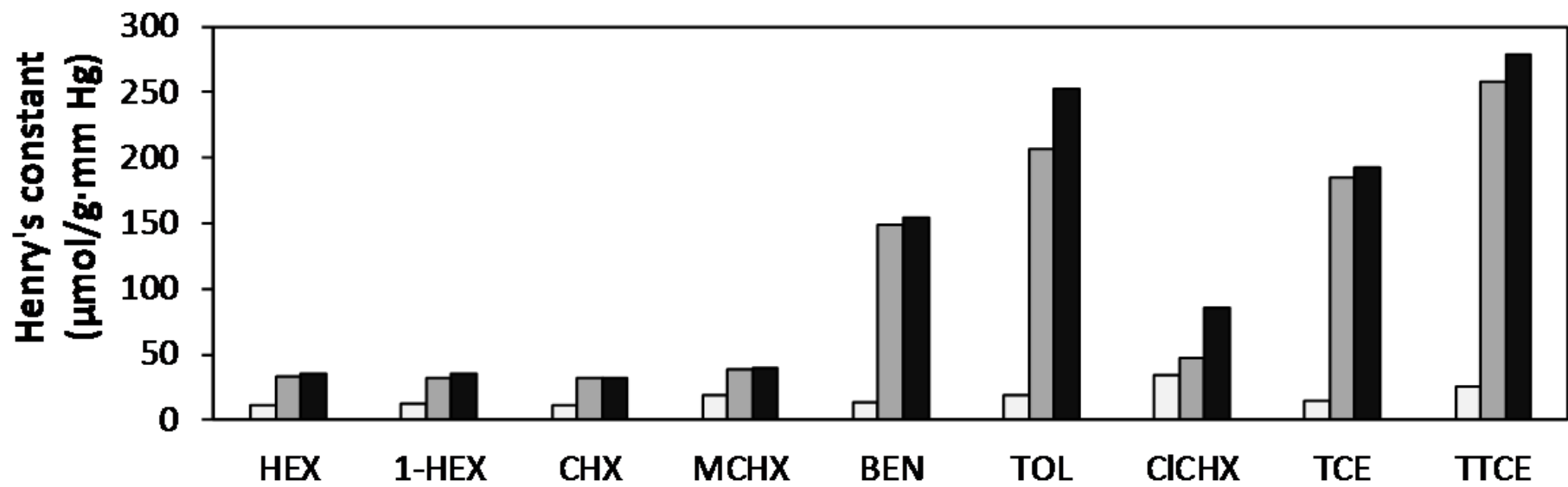
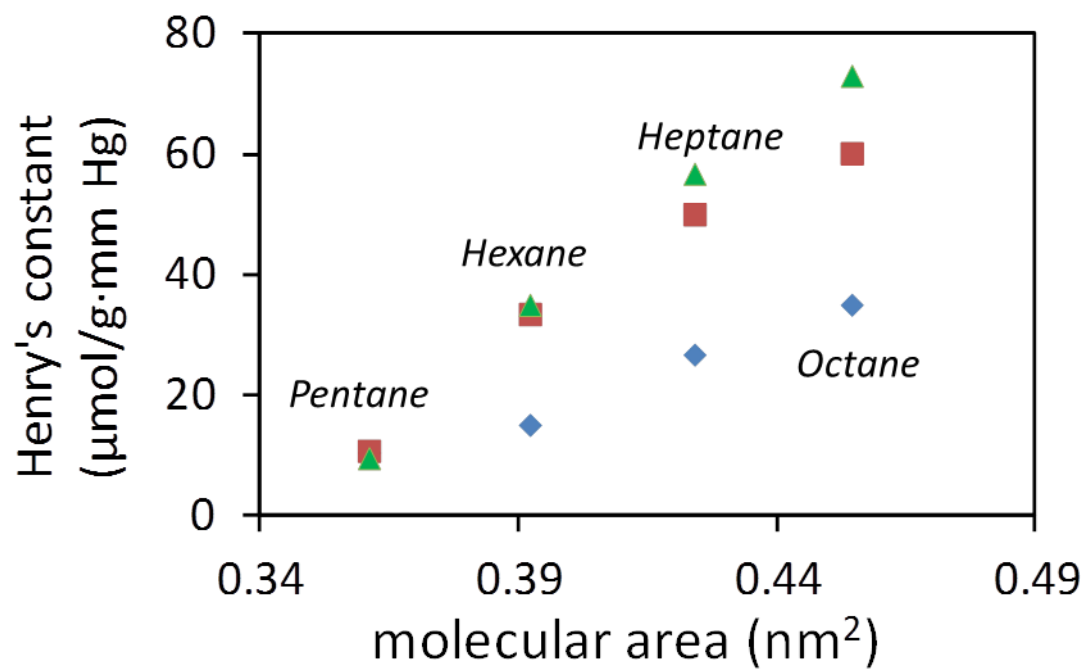


Figure 4.

1
2
3
4
5
6
7



8
9
10
11
12
13
14
15
16
17
18
19
20
21

Figure 5.

22
23
24
25
26
27

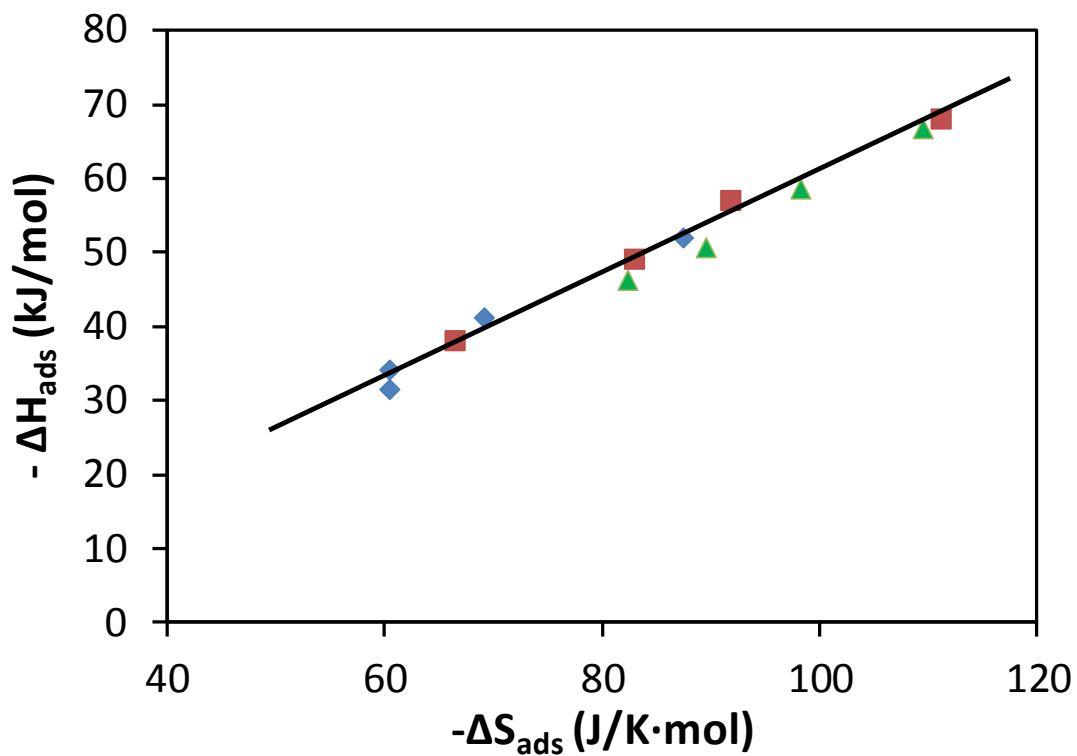
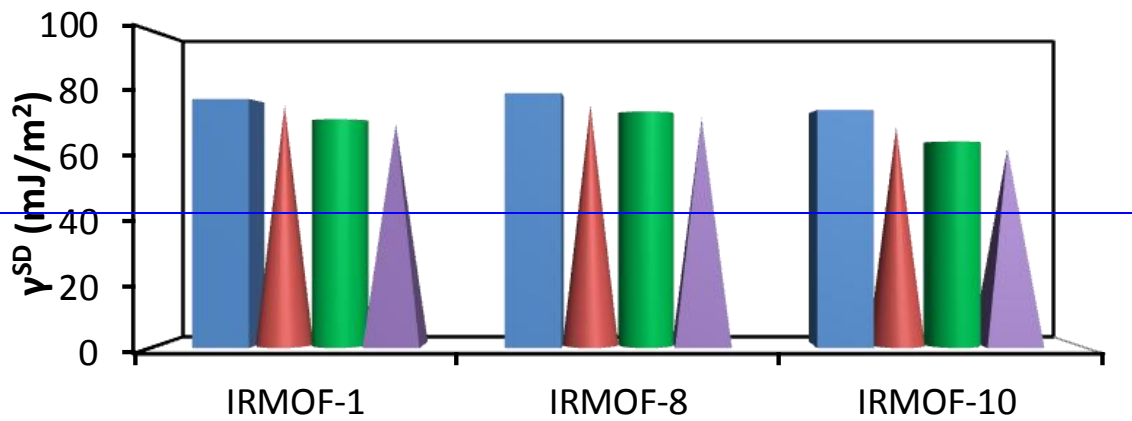


Figure 6.

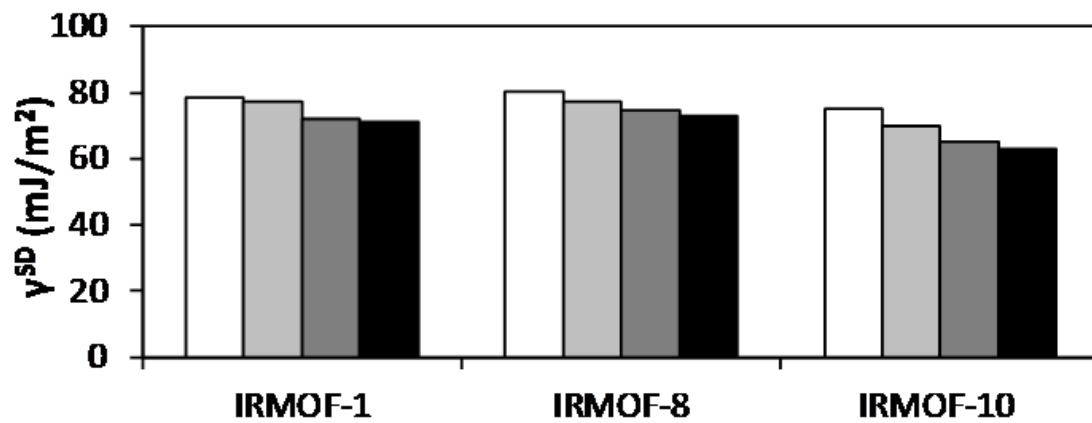
28
29
30
31
32
33
34
35
36
37
38
39
40
41
42

43

44



45



46

47

Figure 7.

48

49

50

51

52

53

54

55

56

57

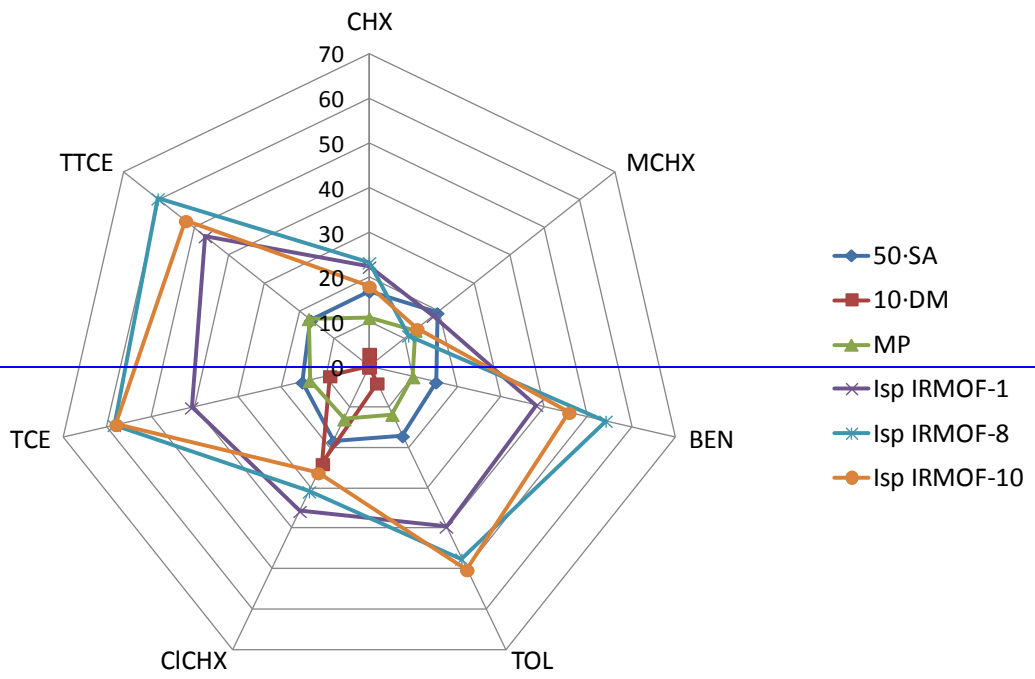
58

59

60

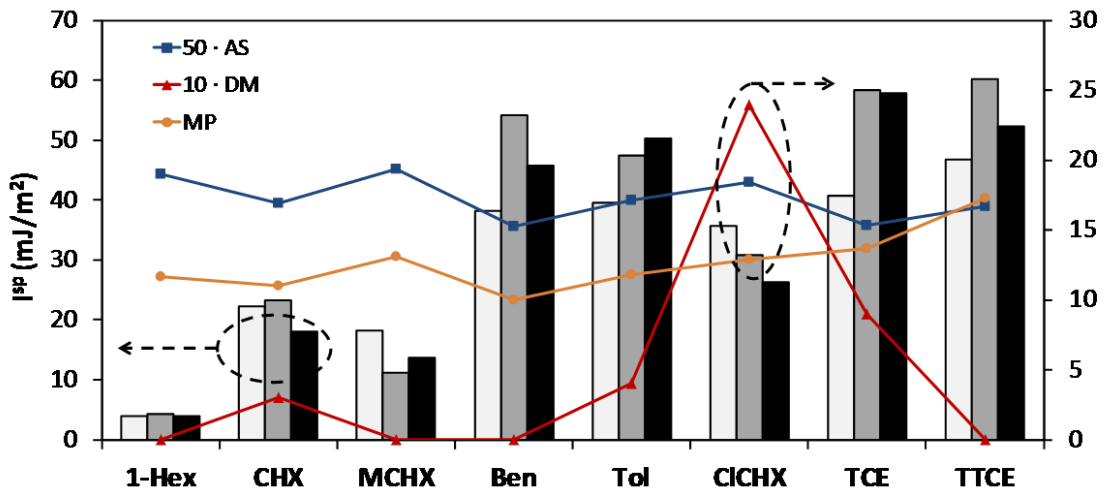
61

62



63

64



65

66

67

68

69

70

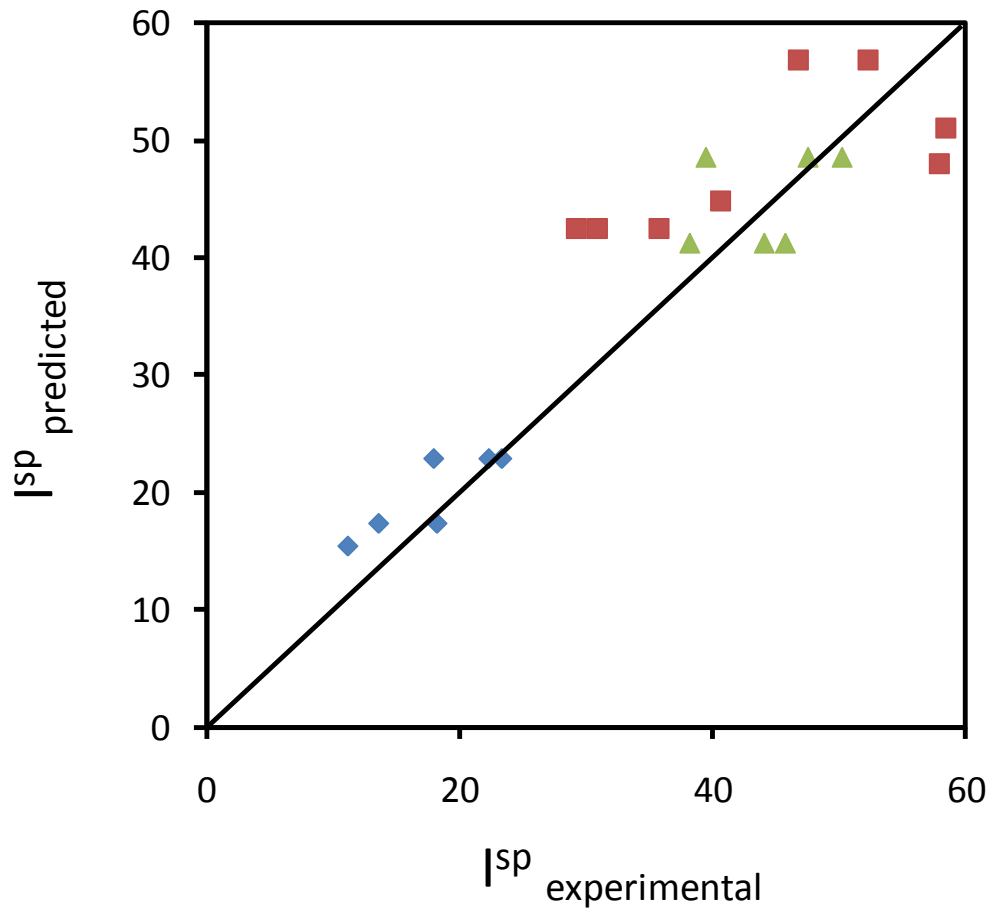
71

72

73

Figure. 8

74
75
76



77
78
79
80

Figure 9.

81
82
83
84
85
86
87
88
89
90
91
92
93
94
95
96
97
98
99
100
101
102
103
104
105
106
107
108
109

Figure captions

Figure 1. XRD patterns for IRMOF-1, IRMOF-8 and IRMOF-10.

Figure 2. N₂ adsorption-desorption isotherms at 77 K for IRMOF-1 (◆), IRMOF-8 (▲) and IRMOF-10 (■). Filled symbols: adsorption and open symbols: desorption.

Figure 3. TG and DTG curves of: (a) IRMOF-1, (b) IRMOF-8 and (c) IRMOF-10. Solid line: TG and broken line: DTG.

Figure 4. Henry's constant at 423 K for *n*-hexane (HEX), 1-hexene (1-HEX), cyclohexane (CHX), methylcyclohexane (MCHX), benzene (BEN), toluene (TOL), trichloroethylene (TCE) and tetrachloroethylene (TTCE) over: IRMOF-1 (rectangle light grey), IRMOF-8 (circle dark grey) and IRMOF-10 (cylinder black).

Figure 5. Relationship between Henry's constants and the molecular area for the *n*-alkanes (IRMOF-1 (◆), IRMOF-8 (▲) and IRMOF-10 (■)).

Figure 6. The thermodynamic compensation effect for: IRMOF-1 (◆), IRMOF-8 (▲) and IRMOF-10 (■).

Figure 7. Dispersive component of the surface free energy of the IRMOFs at several temperatures: 393 K (rectangle white), 403 K (circle light grey), 413 K (cylinder dark grey) and 423 K (pyramid black).

Figure 8. Influence of surface area (SA), dipolar moment (DM) and molecular polarizability (MP) of selected adsorbates on the I^{sp} parameter at 423 K. Follow left axis for I^{sp} and right axis for the other three parameters.

Figure 9. Predicted versus experimental I^{sp} parameter at 423 K for selected compounds, for the three studied adsorbents: IRMOF-1 (◆), IRMOF-8 (▲) and IRMOF-10 (■).